Yang *et al. J. Mater. Inf.* **2025**, *5*, 16
DOI: 10.20517/jmi.2024.79

Journal of Materials Informatics

Research Article

Open Access

Check for updates

Cosolvent-involved hybrid solvation models for aqueous Zn-ion electrolytes: a case study of ethylene glycol-H_2O-$ZnSO_4$ system

Xi Yang, Shichen Sun, Kevin Huang*

Department of Mechanical Engineering, University of South Carolina, Columbia, SC 29201, USA.

***Correspondence to:** Prof. Kevin Huang, Department of Mechanical Engineering, University of South Carolina, 541 Main Street, Columbia, SC 29201, USA. E-mail: huang46@cec.sc.edu

How to cite this article: Yang, X.; Sun, S.; Huang, K. Cosolvent-involved hybrid solvation models for aqueous Zn-ion electrolytes: a case study of ethylene glycol-H_2O-$ZnSO_4$ system. *J. Mater. Inf.* **2025**, *5*, 16. https://dx.doi.org/10.20517/jmi.2024.79

Received: 27 Nov 2024 **First Decision:** 25 Dec 2024 **Revised:** 8 Jan 2025 **Accepted:** 16 Jan 2025 **Published:** 27 Feb 2025

Academic Editor: Hao Li **Copy Editor:** Pei-Yun Wang **Production Editor:** Pei-Yun Wang

Abstract

Tuning electrolyte bulk properties, fundamentally the Zn-ion solvation structures, is key to addressing degradation issues in aqueous Zn-ion batteries (AZIBs). The common practice is to add water-soluble organics as a cosolvent. However, a comprehensive fundamental understanding of the cosolvent effect on electrolyte bulk properties is still lacking. In this work, using ethylene glycol (EG) as the cosolvent and 2M $ZnSO_4$ as the base aqueous Zn-ion electrolyte, we report from a computational perspective how the cosolvent affects aqueous electrolyte bulk properties such as conductivity and pH. To ensure reliability of the computational results, we have used experimental ion conductivity data to validate our computing methods. Further, we show new hybrid solvation models that encompass H_2O, cosolvent and anion, e.g., EG-$Zn(H_2O)_5^{2+}$ and EG-$Zn(H_2O)_4^{2+}$-SO_4^{2-}. Based on these cosolvent-involved Zn-ion solvation models, the experimental pH trending has been successfully explained. Our work offers new insights into the cosolvent effect on aqueous Zn-ion electrolyte bulk properties and solvation structures.

Keywords: Cosolvent-involved hybrid solvation models, 2M $ZnSO_4$, ethylene glycol, pH, conductivity

INTRODUCTION

As a potential battery for commercial large-scale energy storage applications, aqueous Zn-ion batteries

(AZIBs) must overcome critical degradation issues to significantly increase cycle life. The root causes of the degradation in AZIBs are the interactions between aqueous electrolytes and electrodes. At the Zn-anode/electrolyte interface, during the charge cycle, hydrogen evolution reaction (HER) results in a passive surface layer rich in Zn-salt double hydroxides (aka. layered double hydroxides, LDH) and poor in electrical conductivity[1]. Since the formation and dissolution of LDH on the Zn-anode surface is not fully reversible, it results in a gradual LDH buildup, and thus, an increase in resistance. The extent of HER at the anode/electrolyte interface is determined by bulk properties of electrolytes, which are fundamentally rooted in Zn-ion solvation structures. For example, the Zn-ion solvation structure $Zn(H_2O)_6^{2+}$ can release H^+ (i.e., deprotonation) via hydrolysis reactions such as $Zn(H_2O)_6^{2+} + H_2O \rightleftharpoons H_3O^+ + Zn(H_2O)_5(OH)^+$. The H_3O^+ (i.e., H^+, the proton) becomes the driver for HER and the $Zn(H_2O)_5(OH)^+$ becomes a precursor for Zn-salt LDH.

Similarly, LDH formation can also be promoted at the cathode/electrolyte interface during the discharge cycle, as the H^+ derived from Zn-ion solvation structures can co-intercalate with Zn^{2+} into the cathode structure to elevate pH near the cathode surface. However, different from LDH formation at the Zn-anode/electrolyte interface, the LDH formation at the cathode/electrolyte interface is reversible, as H^+ released from the cathode during the charge cycle can redissolve LDH[1-3]. Instead, cathode dissolution is a primary degradation mechanism at the cathode/electrolyte interface[4-8], causing loss of active materials and changes in electrolyte bulk properties.

In the above degradation issues, the bulk properties of electrolytes play a key role. To address the issues, the common practice[9-13] is to tune critical bulk properties (e.g., ion conductivity and pH) of aqueous Zn-salt electrolytes with water-soluble organic molecules. In these cases, the organic molecules become a cosolvent, altering Zn-ion solvation structures through interactions between solvent molecules, ions, and cosolvent molecules. Therefore, the deprotonation ability of Zn-ion solvation structures, i.e., the hydrolysis of Zn^{2+}, is significantly limited. As a result, HER at the anode/electrolyte interface is suppressed, and the Zn anode is protected from H_2O corrosion and LDH formation. On the other hand, since a significant portion of the cathode capacity is contributed from H^+ intercalation, reduced deprotonation of the Zn-ion solvation structures by an inappropriate cosolvent could have a negative effect on the full battery capacity. Similarly, if the cosolvent has a strong affinity with Zn^{2+}, the battery capacity will also be reduced, as the intercalation of Zn^{2+} into the cathode will be impeded due to the high Zn^{2+}-desolvation penalty. Therefore, the identification of a proper cosolvent that forms Zn-ion solvation structures with a balanced deprotonation and Zn^{2+}-desolvation is critically important to achieve high capacity of Zn-ion batteries.

Identifying the best cosolvent requires a fundamental understanding of the cosolvent effect on Zn-ion solvation structures, which is still lacking. To fill this scientific gap, we conduct computational work to investigate how the cosolvent affects bulk properties and alters Zn-ion solvation structures. Ethylene glycol (EG) was chosen as a cosolvent for this study because of its low cost, low volatility, and excellent solubility in water. Most importantly, a significant improvement in Zn-Zn half-cell cycling stability has been reported with the addition of a wide range of EG in 2M $ZnSO_4$ (4 to 68 vol% with the best performance at 40 vol%)[12-14]. However, so far little is known about why and how EG as a cosolvent in aqueous electrolytes influences the AZIB performance. To fill this gap, in this theoretical study, we first validate our computational methodology by comparing our calculated results with experimental data of ionic conductivity. After method validation, we further establish new hybrid solvation models that encompass Zn^{2+}, SO_4^{2-}, H_2O, and cosolvent EG. Using the cosolvent-involved hybrid solvation models, the trend in experimental pH was successfully explained. The limitations of the developed computational methods and possible future work are also discussed.

MATERIALS AND METHODS

Force field parameters for atomistic molecular dynamics simulations

Molecular dynamics (MD) at the atomistic level was performed using GROMACS (2019.6 GPU version)[15]. For water molecules and Zn^{2+}, the Amber03 force field SPC/E model and built-in Zn^{2+} parameters were used, respectively. For SO_4^{2-} and EG, force field parameters were obtained in the following way.

Gaussian 16 software package[16] was used to perform quantum chemistry calculations (structure optimization, frequency analysis, and single point energy calculations) for SO_4^{2-} and EG. For SO_4^{2-}, calculations were performed at the B3LYP/6-311++G(d,p) level of theory, while for EG, calculations were performed at the B3LYP/6-311G(d,p) level without diffuse functions. For single point energy calculations, an implicit solvent model was used by adding the keyword scrf (solvent = water). Following the calculations, the results were processed by Multiwfn[17,18] (version 3.6) and Sobtop[19] (version 1.0 dev3.1) to obtain restrained electrostatic potential[20] (RESP) atomic charges and General Amber Force Field[21] (GAFF) force field parameters for performing atomistic MD.

Atomistic classical MD

All the MD simulations were performed using GROMACS (2019.6 GPU version)[15]. The volume fraction of EG (i.e., the EG concentration, denoted as *f*) varied from 0% to 50%, and the volume sum of EG and water was fixed. Thus, the $ZnSO_4$ concentration was kept the same for systems with different EG volume fractions. In this work, the $ZnSO_4$ concentration is 2M (2 mol/L), as this concentration has been experimentally used in previous works[22,23] and proven to exhibit the highest conductivity[24]. At each EG volume fraction, there were 36 Zn^{2+} ions, 36 SO_4^{2-} ions, water molecules, and EG molecules in a simulation box with three-dimensional periodic boundary conditions. For a system with *f* volume fraction EG, the $ZnSO_4$ concentration is calculated by:

$$c(\mathrm{ZnSO_4}) = \frac{n(\mathrm{ZnSO_4})}{V(EG)+V(W)} = \frac{\frac{36}{N_A}}{\frac{\frac{N_{EG}}{N_A}\cdot M_{EG}}{\rho_{EG}} + \frac{\frac{N_w}{N_A}\cdot M_w}{\rho_w}} = \frac{36}{\left(\frac{N_{EG}\cdot M_{EG}}{\rho_{EG}}\cdot\frac{\rho_w}{M_w} + N_w\right)\cdot\frac{M_w}{\rho_w}} = 2\ \mathrm{mol/L}, \quad (1)$$

where $n(\mathrm{ZnSO_4})$, $V(EG)$, $V(W)$, N_A, N_{EG}, N_w, M_{EG}, M_w, ρ_{EG}, and ρ_w are the amount of $ZnSO_4$, the volume of EG, the volume of water, the Avogadro constant, the number of EG molecules, the number of water molecules, the molar mass of EG, the molar mass of water, the density of EG, and the density of water, respectively.

Thus, we have

$$\frac{N_{EG}\cdot M_{EG}}{\rho_{EG}}\cdot\frac{\rho_w}{M_w} + N_w \approx 1000. \quad (2)$$

and

$$\frac{V(EG)}{V(W)} = \frac{\frac{\frac{N_{EG}}{N_A}\cdot M_{EG}}{\rho_{EG}}}{\frac{\frac{N_w}{N_A}\cdot M_w}{\rho_w}} = \frac{f}{1-f}. \quad (3)$$

Combining Equations (2) and (3), we have

$$N_w = 1000(1 - f) \tag{4}$$

and

$$N_{EG} = 1000 \frac{\frac{M_w}{\rho_w}}{\frac{M_{EG}}{\rho_{EG}}} f \approx 323.22f. \tag{5}$$

N_w and N_{EG} were calculated at each EG volume fraction f; see Supplementary Table 1 for details.

At each f, we first performed an energy minimization (EM) to prevent unphysical particle overlapping. We noticed that inappropriately prepared initial configurations can lead to unphysical aggregation of anions and cations, which results in abnormal deviations in diffusion coefficients. To avoid the deviations, we have ensured that anions and cations are well dispersed in the systems. Then, we performed a 10 ns isothermal-isochoric (NVT) MD simulation at 298.15 K, which was followed by a 40 ns isothermal-isobaric (NPT) MD simulation at 1 atm, 298.15 K. The time step was 0.002 ps. Nosé-Hoover thermostat was used to control the temperature of NVT MD and NPT MD, and Parrinello-Rahman barostat was used to control the pressure of NPT MD. At each f, the last 30 ns NPT MD trajectory was used for result analysis.

Diffusion coefficient and ion conductivity

Based on recent studies on analyzing diffusion coefficients from NPT MD, systematic errors seem to have little effect on analyzing 30 ns-length trajectories[25,26]. Therefore, we directly processed the last 30 ns NPT MD trajectories and calculated the mean squared displacement (MSD). According to the MSD plot in Supplementary Figure 1, we fitted all diffusion coefficients D using the 5,000 ps-to-15,000 ps part of the last 30 ns NPT trajectories [Supplementary Table 2].

The ion conductivity is related to the Nernst-Einstein equation, as given in[27]

$$\sigma = \sum_k \sigma_k = \sum_k \frac{z_k^2 F^2}{RT} c_k D_k, \tag{6}$$

where σ_k, z_k, c_k, and D_k are the conductivity, the charges, the concentration, and the diffusion coefficient of the ion species k; F, R, and T are the Faraday's constant, the ideal gas constant, and temperature, respectively.

In the last 30 ns NPT simulations, the equilibrium volumes of systems with different f are almost the same [Supplementary Figure 2], corresponding to the fixed $ZnSO_4$ concentration c_k of 2M. Thus, for an ion species k, the only variable that governs Equation (6) is D_k. Therefore, we have $\sigma_k \propto D_k$. In addition, for $ZnSO_4$, $z_{Zn^{2+}} = z_{SO_4^{2-}}$, and thus we have $\sigma \propto \sum_k D_k$; i.e., higher conductivities are related to higher diffusion coefficients (faster diffusion).

Radial distribution function and coordination number

GROMACS built-in tools were used to calculate the radial distribution function [RDF, denoted as $g(r)$] between selected atoms. By integrating $g(r)$ over r, we also calculated the average coordination number (CN), denoted as $N(r)$, of selected atoms around a central atom within the distance r, as given in:

$$N(r) = 4\pi\rho \int_0^r r^2 g(r) dr \quad (7)$$

where ρ is the average density of selected atoms.

Hybrid solvation models and deprotonation ability

Gaussian 16 software[16] was used to perform quantum chemistry calculations. Based on the optimized $Zn(H_2O)_6^{2+}$ solvation structure and the CN $N(r)$, we further replaced some water molecules of $Zn(H_2O)_6^{2+}$ by EG or SO_4^{2-} to construct hybrid solvation models. Based on these models, we performed single point energy calculation at the B3LYP/def2-TZVP level and analyzed the deprotonation ability by calculating molecular electrostatic potential on the nucleus of the dissociating proton (MEP_H)[28-30]. Multiwfn[17,18] was used to obtain the MEP_H values of H nuclei in H_2O. For a solvation model, we determined the MEP_H value of the most possible site for proton dissociation. We also compared MEP_H values of different solvation models to explain pH trends.

RESULTS AND DISCUSSION

Cosolvent-ion interactions: ion diffusion and conductivity

Figure 1 shows the individual atomic partial charges for SO_4^{2-}, water, and cosolvent EG. As there are electrostatic interactions between ions, water, and EG, adding EG effectively changes the spatial distribution of ions and molecules. For example, Figure 2A shows a snapshot of EG molecules interacting with water molecules. In Figure 2B, at elevated EG concentrations, increasing EG molecules are dispersed in the electrolyte. Notably, since cosolvent EG has an atomic charge distribution, the dispersed EG molecules can interact with charged ions (SO_4^{2-} and Zn^{2+}). Figure 2C illustrates a snapshot of the local structure of EG interacting with SO_4^{2-} and Zn^{2+}.

The electrostatic interactions between cosolvents and ions can slow down ion diffusion, and thus lower the ion conductivity. Specifically, for the $ZnSO_4$ systems, we have $\sigma \propto \sum_k D_k$ (see Section "Diffusion coefficient and ion conductivity"); i.e., ion conductivity of the electrolyte is proportional to the summation of ion diffusion coefficients. The calculated diffusion coefficients of Zn^{2+} and SO_4^{2-} at elevated EG concentrations are shown in Supplementary Table 2 and plotted in Figure 3A. In Figure 3A, as the EG volume fraction increases, the diffusion coefficients $D(Zn^{2+})$ and $D(SO_4^{2-})$ are found to decrease in general. According to $\sigma \propto \sum_k D_k$, the decrease of $D(Zn^{2+})$ and $D(SO_4^{2-})$ suggests a general decrease in the electrolyte conductivity. Indeed, experimental data in Figure 3B confirm the decrease in the ion conductivity at elevated EG concentrations, proving the cosolvent-ion interactions.

In Figure 3A, some data points deviate from the general trend, e.g., the diffusion coefficients at 30 vol% EG. The deviation may be caused by inappropriate force field parameters and insufficient sampling, as there are strong electrostatic interactions between SO_4^{2-} and Zn^{2+}. In fact, according to our previous study[24], noticeable discrepancies between the calculated conductivity and experimental conductivity were observed for the 2M $ZnSO_4$ electrolyte. In this work, inclusion of additional cosolvent-solvent and cosolvent-ion interactions further increases the difficulty in simulating the 2M $ZnSO_4$ system.

However, even for the difficult 2M $ZnSO_4$ system, the computed trend is in good agreement with the experimental data, demonstrating the capability of our computational methods. At higher Zn-salt concentrations, the stronger electrostatic attractions between Zn^{2+} and SO_4^{2-} slow down ionic diffusion (Walden's rule[31]), while reducing the sampling efficiency and the fidelity of the computation. Instead, other Zn-salt systems containing less negatively charged anions (such as ClO_4^-) at lower concentrations are more likely to be sufficiently sampled with less deviation between model and real experimental systems[24].

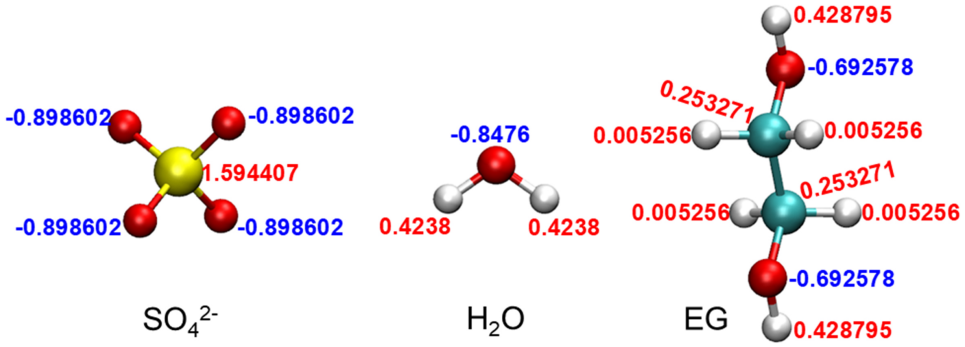

Figure 1. Individual atomic partial charges of SO_4^{2-}, water, and EG. The partial charges of SO_4^{2-} and EG are calculated from the RESP method[20], and the partial charges of H_2O are obtained from GROMACS Amber03 force field SPC/E water model parameters. EG: Ethylene glycol; RESP: restrained electrostatic potential.

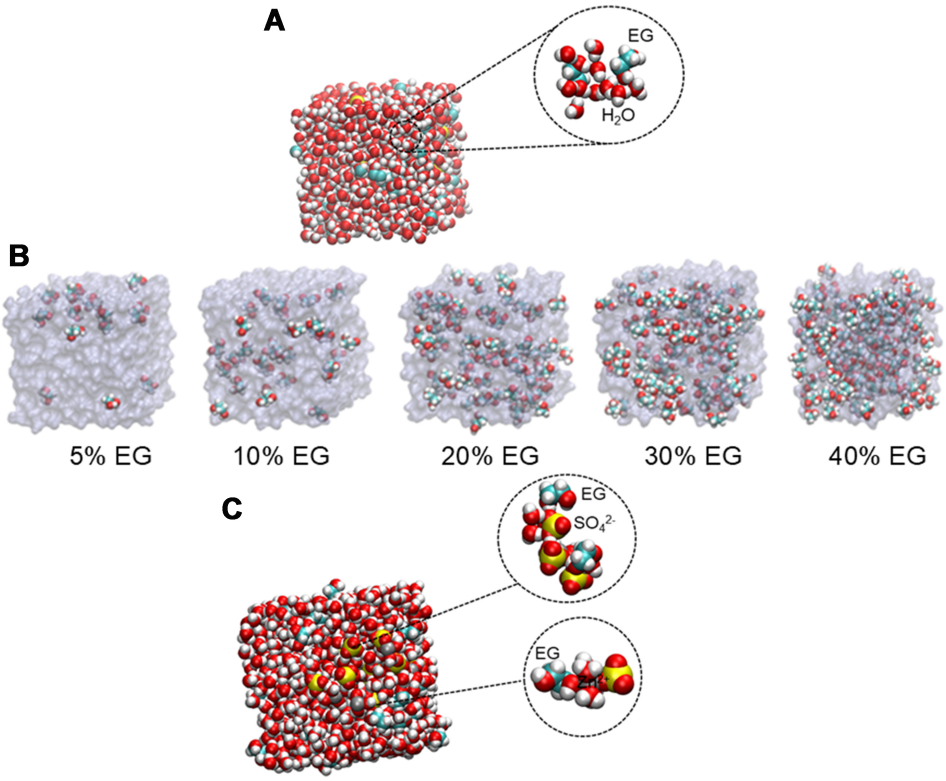

Figure 2. (A) A snapshot of the EG molecules interacting with water molecules; (B) As the EG volume fraction increases from 0% to 40%, EG molecules are found to be more and more spatially dispersed in the electrolyte; (C) A snapshot of local structures of EG molecules interacting with ions (SO_4^{2-} and Zn^{2+}). EG: Ethylene glycol.

Cosolvent-involved hybrid solvation structures

In the previous section, our simulation results are successfully validated by the experimental trend of the ion conductivity. In this section, based on the simulation results, we first derive possible solvation structures by analyzing the structure of solvation shells[32]. Due to EG-Zn^{2+} [Figure 2C] and EG-water interactions [Figure 2A], it is expected that the Zn-ion solvation shell will be altered. Possible solvation shells under the influence of EG can be derived from the $g(r)$ and the $N(r)$. From the $g(r)$ in Figure 4A(i)-D(i), the first coordination shell cut-off r_{cut}(Zn-O) is determined as 0.25 nm. From $g(r)$ in Figure 4E(i), the first

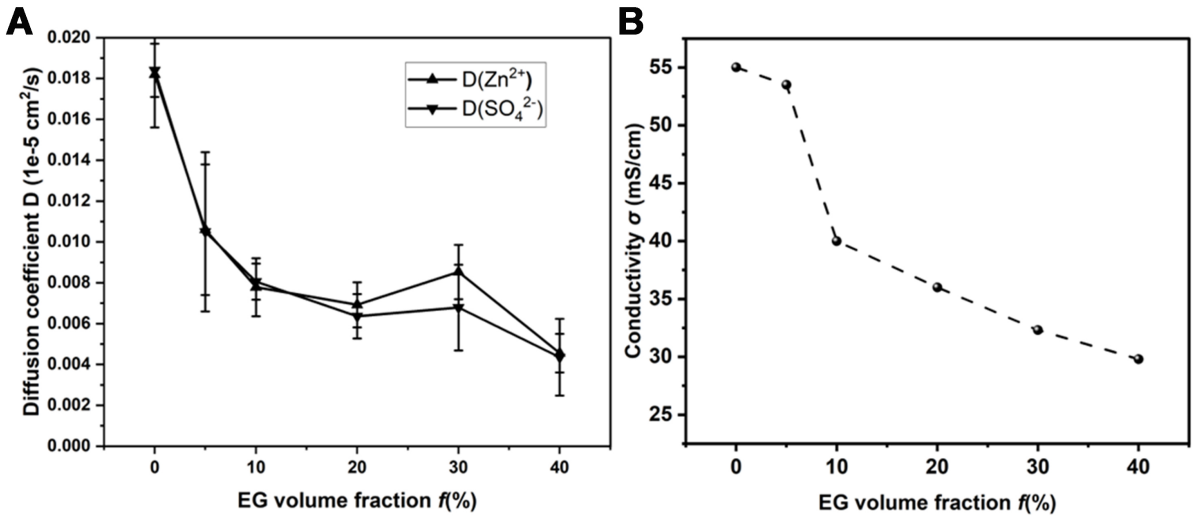

Figure 3. (A) Diffusion coefficients of Zn^{2+} and SO_4^{2-} in electrolytes of different EG volume fractions. As the EG volume fraction increases, the diffusion coefficients are found to decrease in general; (B) Experimental data of the ion conductivity (σ). As the EG volume fraction increases, the ion conductivity decreases. EG: Ethylene glycol.

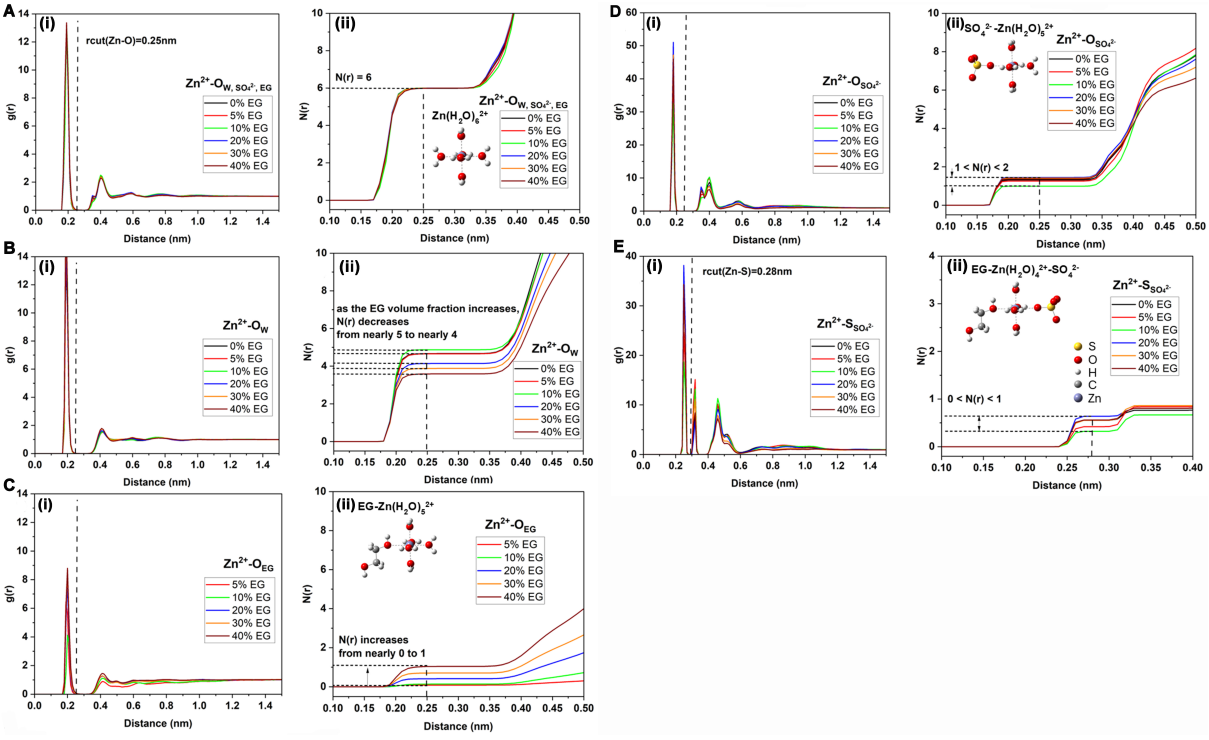

Figure 4. (A-D) The RDF *g*(*r*) and the CN *N*(*r*) of Zn-O pairs. O atoms can be from SO_4^{2-}, EG, water, or all the possible O atoms in the system. The Zn^{2+} first coordination shell cut-off r_{cut}(Zn-O) is found to be 0.25 nm; (E) The *g*(*r*) and the *N*(*r*) of Zn-S pairs. S atoms are from SO_4^{2-}. The Zn^{2+} first coordination shell cut-off r_{cut}(Zn-S) is found to be 0.28 nm. [A(ii)-E(ii)] For the specific type of atoms (all possible O atoms, O_W, O_{EG}, O_{SO4}^{2-}, S_{SO4}^{2-}) around Zn^{2+}, the first shell (i.e., the solvation shell) *N*(*r*) is determined. RDF: Radial distribution function; CN: coordination number; EG: ethylene glycol.

coordination shell cut-off r_{cut}(Zn-S) is determined as 0.28 nm. Note that the atoms that Zn^{2+} can easily coordinate with are the negatively charged O atoms. According to Figure 4A(ii), the O atom CN in the Zn^{2+}

solvation shell is determined to be $N(r) = 6$. Therefore, in Zn-ion solvation structures, there are always six coordinated O atoms from either water, SO_4^{2-}, or EG, which depend on the exact composition of the electrolyte.

Next, from Figure 4B(ii) to 4E(ii), more details about the solvation shell can be obtained. In Figure 4B(ii), as the EG volume fraction increases from 0% to 40%, the $N(r)$ of O_w (O in water) around Zn^{2+} decreases from nearly 5 to nearly 4, indicating other possible solvation structures besides $Zn(H_2O)_6^{2+}$. We also notice that the CN of O_w in water with Zn^{2+} reaches a maximum of 10% EG. While we do not know the exact reason, we suspect that the interaction between EG and SO_4^{2-} reduces the coordination of SO_4^{2-} with Zn^{2+}, thus increasing the coordination with H_2O.

Figure 4C(ii) shows an increased $N(r)$ of O_{EG} (O in EG) from 0 to 1 at elevated EG concentrations. Combining the $N(r)$ values of O_w and O_{EG}, we may derive EG-$Zn(H_2O)_5^{2+}$ to be another possible solvation structure, as illustrated by the schematic solvation model in Figure 4C(ii). The CNs of SO_4^{2-} in the solvation shell are shown in Figure 4D(ii) and E(ii). Notably, the $N(r)$ of $O_{SO_4^{2-}}$ (O in SO_4^{2-}) in Figure 4D(ii) satisfies $1 < N(r) < 2$, the $N(r)$ of O_w in Figure 4B(ii) ranges from 4 to 5, and the total $N(r)$ of O in Figure 4A(ii) is always 6. Therefore, we may derive SO_4^{2-}-$Zn(H_2O)_5^{2+}$ to be another possible solvation structure, as illustrated in Figure 4D(ii). In addition, the $N(r)$ of $S_{SO_4^{2-}}$ (S in SO_4^{2-}) in Figure 4E(ii) ranges between 0 and 1, suggesting that the number of SO_4^{2-} anions in the solvation shell is most likely to be 1 or 0. Considering the $N(r)$ values in Figure 4A(ii)-E(ii), other solvation models may also exist, e.g., EG-$Zn(H_2O)_4^{2+}$-SO_4^{2-}, as shown in Figure 4E(ii). The solvation models $Zn(H_2O)_6^{2+}$ and SO_4^{2-}-$Zn(H_2O)_5^{2+}$ have been proposed and discussed in our previous works[24] for electrolytes without cosolvents. Notably, when the addition of cosolvent EG molecules to electrolytes [Figure 5] leads to the derivation of new hybrid Zn-ion solvation models involving EG, such as EG-$Zn(H_2O)_5^{2+}$ and EG-$Zn(H_2O)_4^{2+}$-SO_4^{2-}.

Explaining pH using the new hybrid solvation models

Based on these derived solvation models, we further analyze their deprotonation ability and try to explain the experimental pH trend qualitatively. For electrolytes without cosolvent EG, only those solvation models without EG are applicable. We compare the deprotonation abilities of solvation models without/with EG in Figure 6A. As shown, by coordinating with the cosolvent EG, the solvation models are less prone to proton loss, which would lead to a lower H^+ concentration, i.e., a higher pH. This qualitative prediction of pH is confirmed by experimental data [Figure 6B]; i.e., as the EG volume fraction rises from 0% to 40%, the pH generally increases. However, some subtle changes in pH cannot be explained by current solvation models, indicating the need for further study. For example, as the EG volume fraction increases from 0% to 10%, the pH rises significantly, but from 10% to 40%, the increase is more gradual. Addressing these variations may require considering other possible solvation models and the impact of cosolvent concentrations.

Limitations of current work and possible future work

The predicted pH increase by cosolvent EG can explain the formation of a significant amount of LDH on the cathode surface [Supplementary Figure 3], as pH exceeds ~5.1, a value that precipitates out LDH. In addition, Figure 4B(ii)-D(ii) implies that EG increases the difficulty of desolvating Zn^{2+}, which could lead to the accumulation of Zn^{2+}-related chemical species at the cathode-electrolyte interface and result in cathode LDH formation. To fully understand the cosolvent effect on cathode LDH formation, however, further investigations are needed, as there are other complex interfacial effects (e.g., external electric fields) that are beyond the current scope of Zn-ion solvation structures in bulk electrolytes.

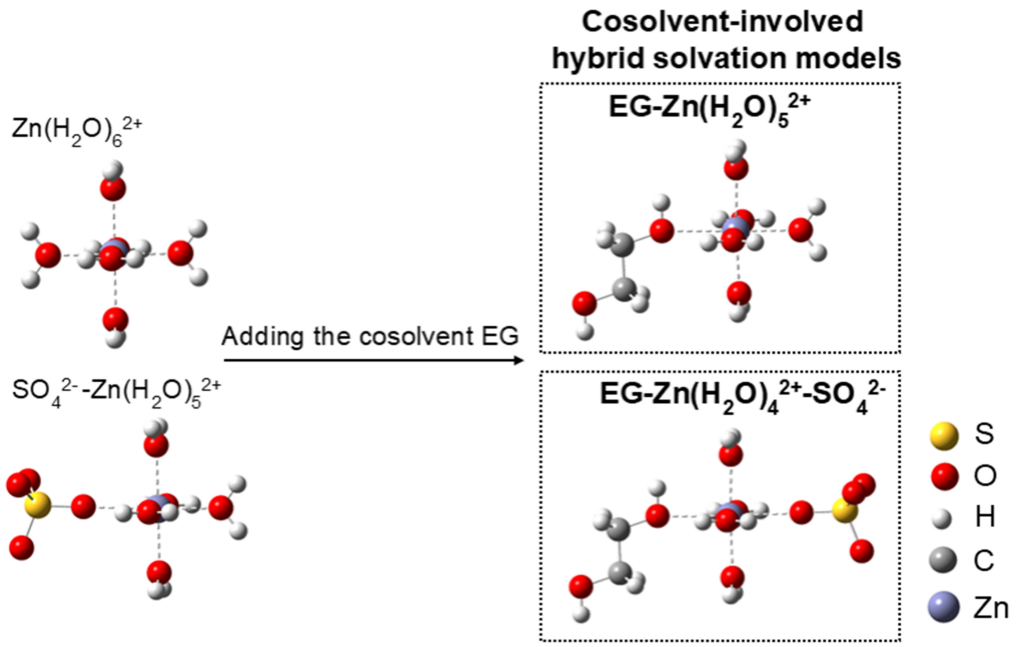

Figure 5. Solvation models derived from Figure 4. After adding EG, there are new hybrid solvation models that involve cosolvent EG. EG: Ethylene glycol.

On the other hand, Figure 4D suggests the existence and dominance of contacting ion pair (CIP)[33-35] in bulk electrolytes, as the $g(r)$ shows that $O_{SO_4^{2-}}$ atoms are more likely to stay in the first shell to coordinate with Zn^{2+} and the first shell CN $N(r)$ is larger than 1. Since there are strong electrostatic attractions between Zn^{2+} and SO_4^{2-}, it is possible that Zn^{2+} and SO_4^{2-} "touch" each other. However, whether CIPs are dominant requires further studies, as there are discrepancies between experiments and computations[24] possibly caused by the inaccurate force field parameters for 2M $ZnSO_4$. There are also sampling problems caused by strong $Zn^{2+}\text{-}SO_4^{2-}$ electrostatic attraction and high salt concentrations. In the future, we plan to study Zn-salt electrolytes with less negatively charged anions (e.g., ClO_4^- and $CF_3SO_3^-$) at slightly lower salt concentrations to get sufficiently sampled and experimentally validated data for investigating CIPs.

CONCLUSIONS

To conclude, using EG as an exemplar cosolvent and 2M $ZnSO_4$ as the base aqueous Zn-ion electrolyte, we have studied the electrolyte bulk properties (conductivity and pH) and derived new hybrid solvation models that encompass Zn^{2+}, SO_4^{2-}, H_2O, and the cosolvent EG. Computational results are validated by experimental data of the ion conductivity. Adding cosolvent EG slows down ion diffusion and causes a decrease in ion conductivity. From the validated computational results, we have also derived new many-body hybrid solvation models, e.g., $EG\text{-}Zn(H_2O)_5^{2+}$ and $EG\text{-}Zn(H_2O)_4^{2+}\text{-}SO_4^{2-}$. Based on these cosolvent-involved Zn-ion solvation models, the experimental pH trend at elevated EG concentrations has been successfully explained, confirming our new hybrid solvation models. Developing more robust solvation models is needed in future work to explain the subtle changes in pH induced by EG cosolvent.

From the computational and experimental results, HER is expected to be effectively suppressed by higher EG concentration. However, too high an EG concentration would result in much retarded cathodic kinetics. Therefore, there exists an optimal EG concentration (likely < 10 vol%) that balances anodic and cathodic kinetics.

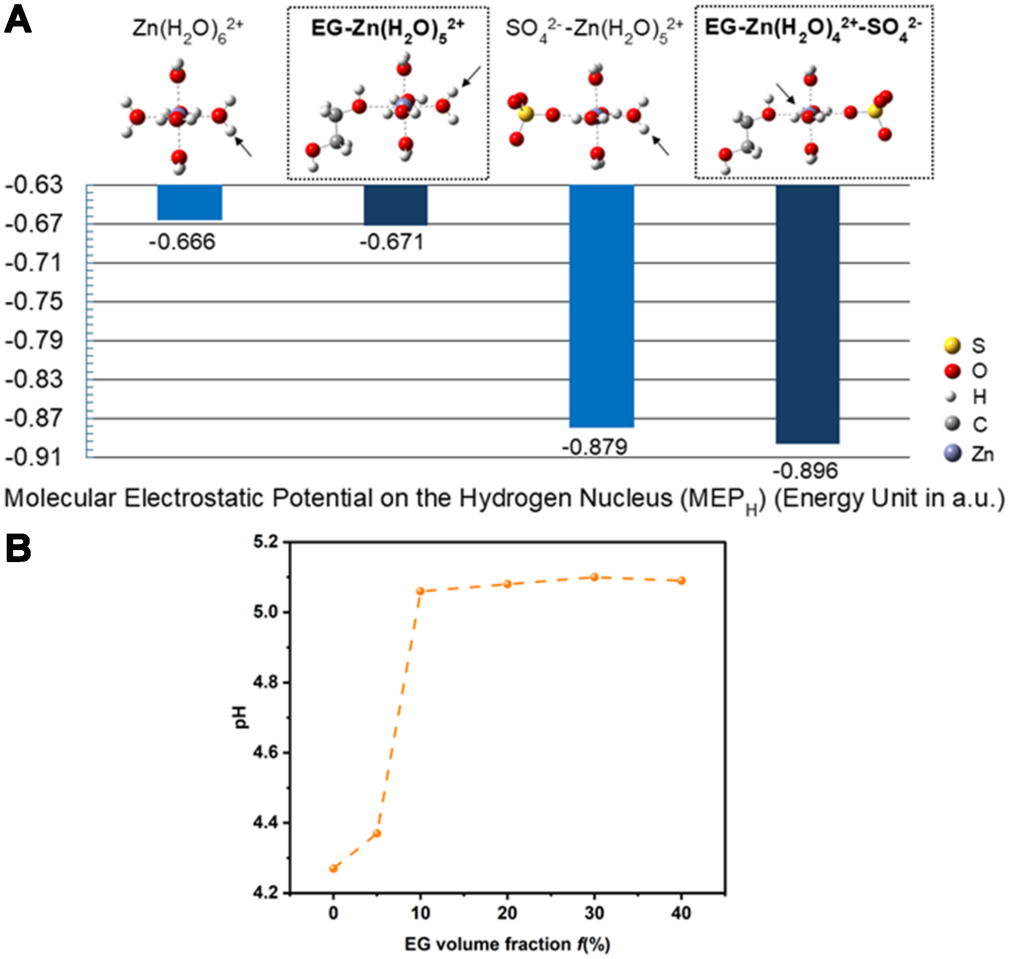

Figure 6. (A) Comparing deprotonation ability of solvation models without/with the cosolvent EG. A more negative MEP_H value corresponds to a lower deprotonation ability or higher pH. Generally, after coordinating with the cosolvent EG, a slight decrease in the MEP_H value is observed for solvation models $EG\text{-}Zn(H_2O)_5^{2+}$ and $EG\text{-}Zn(H_2O)_4^{2+}\text{-}SO_4^{2-}$, indicating that deprotonation becomes more difficult; (B) Experimental values of pH. As the EG volume fraction increases from 0% to 40%, the pH generally increases. EG: Ethylene glycol.

To verify the computational results obtained from this study, more experiments such as Raman spectroscopy, Fourier Transformation Infrared spectroscopy, and water activity measurement should be performed on the bulk properties of the cosolvent electrolytes. Since there is abundant literature supporting EG cosolvent as a suppressor to HER, future research should focus on cathodic kinetics to delineate the deactivation mechanisms. On the other hand, to confirm the existence and dominance of CIPs, further investigations are also required. Our current work provides new computational insights into the cosolvent effect on bulk properties and solvation structures of aqueous Zn-ion electrolytes, laying the foundation for more robust solvation models in the future.

DECLARATIONS

Authors' contributions

Computational modeling, manuscript drafting: Yang, X.
Experimental data collection: Sun, S.

Conception of the idea, manuscript revision: Huang, K.

Availability of data and materials

The data that support the findings of this study are available from the corresponding author upon reasonable request.

Financial support and sponsorship

Research was sponsored by the U.S. Army Research Office (ARO) and was accomplished under Grant Number: W911NF-21-1-0308 and FA9550-23-1-0505. The views and conclusions contained in this document are those of the authors and should not be interpreted as representing the official policies, either expressed or implied, of ARO or the U.S. Government. The U.S. Government is authorized to reproduce and distribute reprints for Government purposes notwithstanding any copyright notation herein.

Conflicts of interest

Huang, K. is an Associate Editor of *Journal of Materials Informatics*. He was not involved in any steps of the editorial process, including reviewer selection, manuscript handling, or decision-making. The other authors declare no conflicts of interest.

Ethical approval and consent to participate

Not applicable.

Consent for publication

Not applicable.

REFERENCES

1. Rajabi, R.; Sun, S.; Billings, A.; Mattick, V. F.; Khan, J.; Huang, K. Insights into chemical and electrochemical interactions between Zn anode and electrolytes in aqueous Zn−ion batteries. *J. Electrochem. Soc.* **2022**, *169*, 110536. DOI
2. Pan, H.; Shao, Y.; Yan, P.; et al. Reversible aqueous zinc/manganese oxide energy storage from conversion reactions. *Nat. Energy.* **2016**, *1*, BFnenergy201639. DOI
3. Guo, X.; Zhou, J.; Bai, C.; Li, X.; Fang, G.; Liang, S. Zn/MnO_2 battery chemistry with dissolution-deposition mechanism. *Mater. Today. Energy.* **2020**, *16*, 100396. DOI
4. Lu, Y.; Zhu, T.; van, B. W.; Stefik, M.; Huang, K. A high performing Zn-ion battery cathode enabled by in situ transformation of V_2O_5 atomic layers. *Angew. Chem. Int. Ed. Engl.* **2020**, *59*, 17004-11. DOI
5. Wang, L.; Huang, K. W.; Chen, J.; Zheng, J. Ultralong cycle stability of aqueous zinc-ion batteries with zinc vanadium oxide cathodes. *Sci. Adv.* **2019**, *5*, eaax4279. DOI PubMed PMC
6. Zhao, W.; Kong, Q.; Wu, X.; et al. ε-MnO_2@C cathode with high stability for aqueous zinc-ion batteries. *Appl. Surf. Sci.* **2022**, *605*, 154685. DOI
7. Chen, C.; Shi, M.; Zhao, Y.; Yang, C.; Zhao, L.; Yan, C. Al-intercalated MnO_2 cathode with reversible phase transition for aqueous Zn-ion batteries. *Chem. Eng. J.* **2021**, *422*, 130375. DOI
8. Li, G.; Sun, L.; Zhang, S.; et al. Developing cathode materials for aqueous zinc ion batteries: challenges and practical prospects. *Adv. Funct. Mater.* **2024**, *34*, 2301291. DOI
9. Wu, F.; Chen, Y.; Chen, Y.; et al. Achieving highly reversible zinc anodes via N, N-dimethylacetamide enabled Zn-ion solvation regulation. *Small* **2022**, *18*, e2202363. DOI
10. Hao, J.; Yuan, L.; Ye, C.; et al. Boosting zinc electrode reversibility in aqueous electrolytes by using low-cost antisolvents. *Angew. Chem. Int. Ed. Engl.* **2021**, *60*, 7366-75. DOI
11. Hou, Z.; Tan, H.; Gao, Y.; Li, M.; Lu, Z.; Zhang, B. Tailoring desolvation kinetics enables stable zinc metal anodes. *J. Mater. Chem. A.* **2020**, *8*, 19367-74. DOI
12. Qin, R.; Wang, Y.; Zhang, M.; et al. Tuning Zn^{2+} coordination environment to suppress dendrite formation for high-performance Zn-

ion batteries. *Nano. Energy.* **2021**, *80*, 105478. DOI

13. Chang, N.; Li, T.; Li, R.; et al. An aqueous hybrid electrolyte for low-temperature zinc-based energy storage devices. *Energy. Environ. Sci.* **2020**, *13*, 3527-35. DOI
14. Jia, H.; Jiang, X.; Wang, Y.; Lam, Y.; Shi, S.; Liu, G. Hybrid Co□solvent□induced high□entropy electrolyte: regulating of hydrated Zn^{2+} solvation structures for excellent reversibility and wide temperature adaptability. *Adv. Energy. Mater.* **2024**, *14*, 2304285. DOI
15. Zenodo. GROMACS 2019.6 Source code. 2020. DOI
16. Gaussian 16. 2016. https://gaussian.com/gaussian16/. (accessed 2025-02-07).
17. Lu, T.; Chen, F. Multiwfn: a multifunctional wavefunction analyzer. *J. Comput. Chem.* **2012**, *33*, 580-92. DOI
18. Lu, T. A comprehensive electron wavefunction analysis toolbox for chemists, Multiwfn. *J. Chem. Phys.* **2024**, *161*, 082503. DOI
19. Sobtop: A tool of generating forcefield parameters and GROMACS topology file. http://sobereva.com/soft/Sobtop. (accessed 2025-02-07)
20. Bayly, C. I.; Cieplak, P.; Cornell, W.; Kollman, P. A. A well-behaved electrostatic potential based method using charge restraints for deriving atomic charges: the RESP model. *J. Phys. Chem.* **1993**, *97*, 10269-80. DOI
21. Wang, J.; Wolf, R. M.; Caldwell, J. W.; Kollman, P. A.; Case, D. A. Development and testing of a general amber force field. *J. Comput. Chem.* **2004**, *25*, 1157-74. DOI
22. Jiang, Y.; Wan, Z.; He, X.; Yang, J. Fine-tuning electrolyte concentration and metal-organic framework surface toward actuating fast Zn^{2+} dehydration for aqueous Zn-ion batteries. *Angew. Chem. Int. Ed. Engl.* **2023**, *62*, e202307274. DOI
23. Yue, J.; Chen, S.; Yang, J.; et al. Multi-ion engineering strategies toward high performance aqueous zinc-based batteries. *Adv. Mater.* **2024**, *36*, e2304040. DOI
24. Sun, S.; Yang, X.; Billings, A.; Huang, K. Understanding the critical bulk properties of Zn-salt solution electrolytes for aqueous Zn-ion batteries. *Chem. Mater.* **2024**, *36*, 6805-15. DOI
25. Bullerjahn, J. T.; von, B. S.; Heidari, M.; Hénin, J.; Hummer, G. Unwrapping NPT simulations to calculate diffusion coefficients. *J. Chem. Theory. Comput.* **2023**, *19*, 3406-17. DOI PubMed PMC
26. von Bülow S, Bullerjahn JT, Hummer G. Systematic errors in diffusion coefficients from long-time molecular dynamics simulations at constant pressure. *J. Chem. Phys.* **2020**, *153*, 021101. DOI PubMed
27. Huang, K.; Goodenough, J. B. Transport of charged particles in a solid oxide fuel cell (SOFC). In: Solid oxide fuel cell technology. Elsevier; 2009. pp. 41-66. https://books.google.com/books?hl=zh-CN&lr=&id=c46kAgAAQBAJ&oi=fnd&pg=PP1&dq=Solid+oxide+fuel+cell+technology.&ots=BaY0QiCZiL&sig=Vj11zv61FcxKTCHjzITGhj9uVXo#v=onepage&q=Solid%20oxide%20fuel%20cell%20technology.&f=false. (accessed 2025-02-07).
28. Cao, X.; Rong, C.; Zhong, A.; Lu, T.; Liu, S. Molecular acidity: an accurate description with information-theoretic approach in density functional reactivity theory. *J. Comput. Chem.* **2018**, *39*, 117-29. DOI
29. Liu, S.; Pedersen, L. G. Estimation of molecular acidity via electrostatic potential at the nucleus and valence natural atomic orbitals. *J. Phys. Chem. A.* **2009**, *113*, 3648-55. DOI PubMed PMC
30. Liu, S.; Schauer, C. K.; Pedersen, L. G. Molecular acidity: a quantitative conceptual density functional theory description. *J. Chem. Phys.* **2009**, *131*, 164107. DOI PubMed PMC
31. Szwajczakaf, E.; Szymański, A. On the relation between mobility of lons and viscosity. the Walden's Rule. *Mol. Cryst. Liq. Cryst.* **1986**, *139*, 253-61. DOI
32. Wang, J.; Zhang, J.; Wu, J.; et al. Interfacial "single-atom-in-defects" catalysts accelerating Li^{+} desolvation kinetics for long-lifespan lithium-metal batteries. *Adv. Mater.* **2023**, *35*, e2302828. DOI
33. Elliott, G. R.; Wanless, E. J.; Webber, G. B.; Andersson, G. G.; Craig, V. S. J.; Page, A. J. Dynamic ion correlations and ion-pair lifetimes in aqueous alkali metal chloride electrolytes. *J. Phys. Chem. B.* **2024**, *128*, 7438-44. DOI PubMed
34. Yu, X.; Chen, M.; Li, Z.; et al. Unlocking dynamic solvation chemistry and hydrogen evolution mechanism in aqueous zinc batteries. *J. Am. Chem. Soc.* **2024**, *146*, 17103-13. DOI
35. Zhang, H.; Ning, F.; Guo, Y.; et al. Unraveling the mechanisms of aqueous zinc ion batteries via first-principles calculations. *ACS. Energy. Lett.* **2024**, *9*, 4761-84. DOI